Predissociation and pressure dependence in the low frequency far wing of the Wulf absorption band of ozone near 1.2 μm

Semen Vasilchenko, Didier Mondelain, Samir Kassi, Alain Campargue

Predissociation and pressure dependence in the low frequency far wing of the Wulf absorption band of ozone near 1.2 µm

Semen Vasilchenko[1,2,3], Didier Mondelain[1], Samir Kassi[1], and Alain Campargue[1,*]

[1] *Université Grenoble Alpes, CNRS, LIPhy, 38000 Grenoble, France*
[2] *V. E. Zuev Institute of Atmospheric Optics SB RAS, av. 1, Akademician Zuev square, 634055 Tomsk, Russia*
[3]*Laboratory of Quantum Mechanics of Molecules and Radiative Processes, Tomsk State University, 36 Lenin Avenue, 634050 Tomsk, Russia*

Number of pages: 25 11 March 2021

Number of tables: 1

Number of figures: 8

Key words: ozone; O3; Wulf band; predissociation

* Corresponding author: alain.campargue@univ-grenoble-alpes.fr

Abstract

The weak low frequency tail of the ozone Wulf band is newly studied by high sensitivity cavity ring down spectroscopy (CRDS) in the 7920-8700 cm^{-1} range. Although strongly obscured by impurity lines, the ozone absorption signature shows up in the recorded spectra as two mostly unresolved absorption bands. These two bands with maximum near 8154 and 8450 cm^{-1} are hot bands from the (020) and (100) ground state vibrational levels reaching the same predissociated $^3A_2(000)$ upper state of $^{16}O_3$. The observed bands include a mostly structureless continuum and lines exhibiting a clear broadening due to the predissociation of the $^3A_2(0\ 0\ 0)$ upper state. On the basis of assignments available in the literature for the $^3A_2(000)$-$X^1A_1(000)$ cold band near 9520 cm^{-1}, about sixty relatively narrow lines could be rotationally assigned to the $^3A_2(000)$-$X^1A_1(020)$ and $^3A_2(000)$-$X^1A_1(100)$ hot bands. A line shape analysis provided the width of the Lorentzian component of their Voigt profile. Additional recordings performed at various pressures for 18 lines allowed to disentangle the pressure and predissociation contributions to the fitted Lorentzian widths. As a result, the newly derived pressure broadening coefficients of the considered rovibronic transitions are found to be similar to those of the rovibrational infrared bands. All the lines studied are affected by significant predissociation due the spin-orbit coupling between the $^3A_2(0\ 0\ 0)$ level and high lying dissociative vibrational levels of the X^1A_1 electronic ground state. The resulting set of predissociation widths for sixty lines ranges between 9×10^{-3} and 0.2 cm^{-1} corresponding to upper state life time of 560 and 25 ps, respectively. The reported results are discussed in relation with previous experimental and theoretical studies.

1. Introduction

Ozone formation and depletion play a key role in various physical and chemical atmospheric processes which remain to be understood at the molecular level [Fabian2014, Schinke2006, Charlo2004, Xie2005, Feilberg2013, Lu2009]. The spectral region near the dissociation threshold, D_0, evaluated around 8560 cm^{-1} from thermochemical measurements by Ruscic et al. [Ruscic2010] presents a high interest as the near-threshold states are expected to play a role in the $O+O_2 \rightarrow O_3$ kinetics and in isotopic exchange reactions [Anderson1985, Janssen2003, Schinke2006, Guillon18, Yuen2019]. In particular, the highly excited rovibrational states approaching D_0 provide an ideal probe of the X^1A_1 ground state potential energy surface computed by *ab initio* calculations [Tyuterev2013, Tyuterev2014] and the effects of interactions among potential wells [Kokoulin2020, Vasilchenko2020]. Nevertheless, the sharp decrease of the intensity of vibrational combination and overtone bands with the energy makes their detection particularly challenging. During the last decade, we have used the cavity-ring-down spectroscopy (CRDS) technique to probe quantum rovibrational states towards the dissociation threshold. The high sensitivity spectra of the main ozone isotopologue, $^{16}O_3$, of $^{18}O_3$, and of various $^{16}O/^{18}O$ mixed isotopologues were recorded and rovibrationally assigned in the 5700-8300 cm^{-1} region [Campargue2006, De Backer-Barilly2006, Barbe2007a, Kassi2007, Barbe2007b, Campargue2008, Mondelain2013, Barbe2011, De Backer-Barilly2012, Barbe2013, Tyuterev2014, Campargue2015, Starikova2015, Vasilchenko2020]. The exceptional sensitivity of the CRDS technique allowed for the detection of the most excited absorption vibrational bands of ozone reported so far, with a band intensity smaller by about 9 orders of magnitude compared to the well-known ν_1 band near 10 µm. As a result, some ground state rovibrational energy levels of $^{16}O_3$ located only 3.3 % below the dissociation threshold could be determined from the analysis [Vasilchenko2020].

In fact, above 8000 cm^{-1}, the main contribution to the ozone spectrum at room temperature is not due to the very weak vibrational bands within the ground electronic state X^1A_1 but to a series of vibronic hot bands forming the low frequency tail of the Wulf band pointing to the excited triplet electronic state $^3A_2$. This finding was first reported during our CRDS study of the spectrum of heavy ozone isotopologue $^{18}O_3$ near 7900 cm^{-1} where unexpected broad absorption lines with intensity quickly increasing with temperature (a factor of 2 for a 30 K increase around room temperature) were observed superimposed to weak vibrational bands [Mondelain2011]. The observed $^{18}O_3$ lines were assigned to the $^3A_2(000) \leftarrow X^1A_1(110)$ hot band with the vibrational energy of the lower state $(\nu_1\nu_2\nu_3)$ =(110) around 1696 cm^{-1} and thus a relative population of only 2.5×10^{-4} at room temperature [Mondelain2012].

The energy diagram of the first vibrational levels of the X^1A_1 ground and $^3A_2$ triplet states of $^{16}O_3$ is presented in **Fig. 1**. The $^3A_2(000) \leftarrow X^1A_1(000)$ cold band with an origin near 9553 cm^{-1} is the first band of the $^3A_2(0\nu_20) \leftarrow X^1A_1(000)$ dominant progression of the Wulf band which shows up as diffuse vibronic bands

from the vibrational ground state, regularly spaced by about 530 cm^{-1} [Anderson1995, Bouvier1998, Grebenshchikov2007, Serdyuchenko2014]. Towards its absorption maximum near 14000 cm^{-1}, the Wulf progression is obscured by the low-energy wing of the much stronger Chappuis band.

As concerns the hot bands under study, they are located significantly below the $^3A_2(000)$-$X^1A_1(000)$ cold band. They correspond to the excitation of the same $^3A_2(000)$ upper state as the cold band but from rovibrational levels of X^1A_1 (100) and X^1A_1 (020). The small population of their lower energy level is only partially compensated by the value of their Franck-Condon (FC) factors which results in smaller band intensities, with respect to the cold band. In Ref. [Mondelain2011], some very weak absorption features of the $^3A_2(000)$-$X^1A_1(110)$ hot band were identified in the CRDS spectrum of $^{16}O_3$ near 7760 cm^{-1} but the weakness of this band (the relative population of the lower lever at 1796 cm^{-1} is about 2×10^{-4}) and the accidental superposition to a stronger vibrational band prevented detailed line profile analysis. According to **Fig. 1**, the hot bands from the more populated (020) and (100) ground electronic state levels at 1399 and 1103 cm^{-1}, respectively, are predicted at 8154 and 8450 cm^{-1}, respectively, and then located in the range of the present recordings (7920-8700 cm^{-1}).

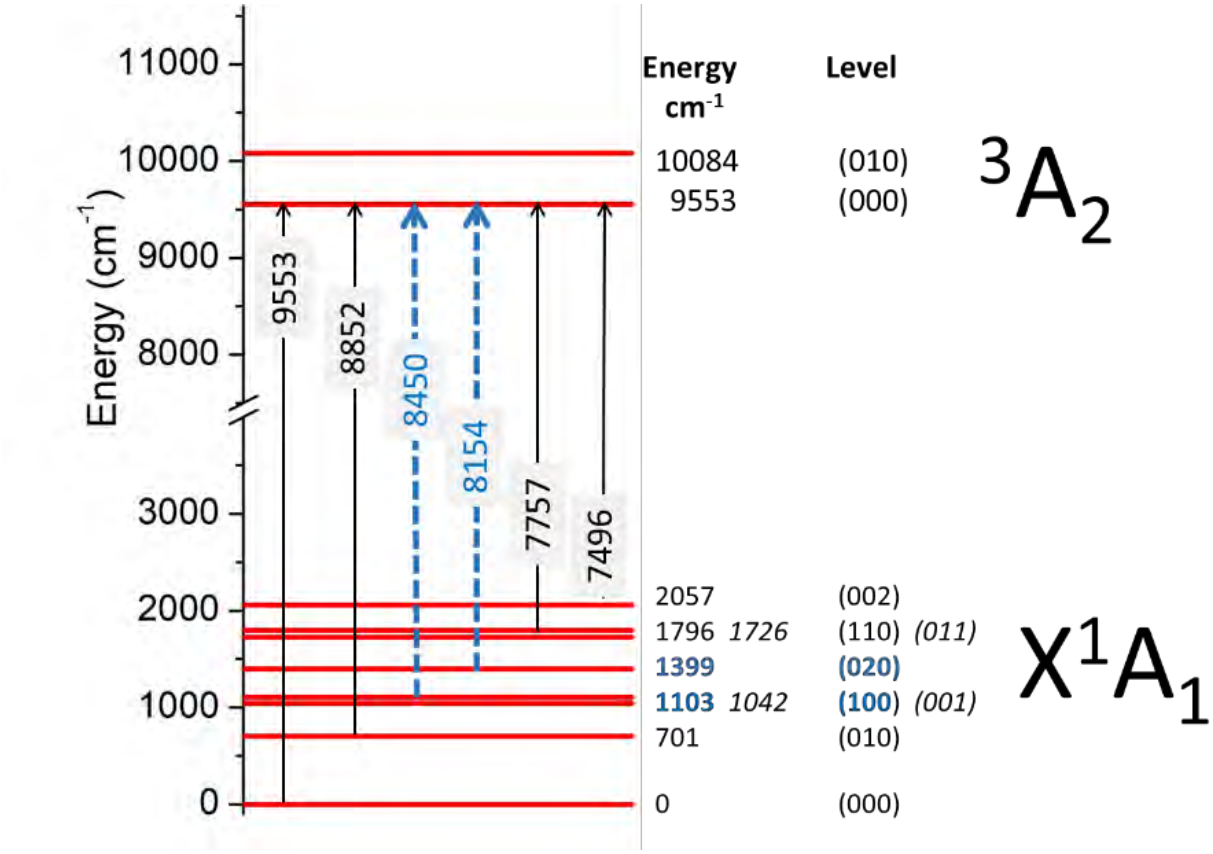

Fig. 1.

Energy diagram for the X^1A_1 electronic ground state and the $^3A_2$ triplet state of $^{16}O_3$. The vibrational energies of the first vibration states of the X^1A_1 state were taken from the SMPO database [Babikov2014]. The two blue arrows show the $^3A_2(000)$-X^1A_1 analyzed hot bands from the (020) and (100) lower states, centered near 8154 and 8450 cm^{-1}, respectively.

It is worth mentioning that the cold band of $^{16}O_3$ near 9553 cm^{-1} shows a partly resolved rotational structure which was previously studied by Fourier transform spectroscopy (FTS) [Bouvier1998, Bouvier1999, Inard1998] and by high sensitivity laser techniques, namely intracavity laser absorption spectroscopy (ICLAS) [Abel1997] and pulsed-cavity ring down Spectroscopy (CRDS) [Wachsmuth2003] These previous studies are of particular interest for the present work as the cold band and the considered hot bands share the same $^3A_2(000)$ upper levels. In particular, the predissociation of the upper state contributes to the observed line widths allowing for life time measurements which may give interesting insights on the coupling mechanism of the $^3A_2$ state with the high lying rovibrational resonant levels of the ground electronic state [Mondelain2012]. The hot bands provide thus an independent way to determine the lifetimes of the $^3A_2(000)$ predissociative states which can thus be compared to the results derived from the cold band analysis [Inard1998, Wachsmuth2003]. The comparison will concern in particular the smallest line widths corresponding to the longest lifetime of the upper levels, for which the presently used CRDS technique provides a higher resolution than the FTS, ICLAS and pulsed CRDS setups used for the cold band studies.

The rest of the papers is organized as follows. In the next paragraph, we will present the experimental setup used to record, for the first time, the ozone spectrum in the 7920-8700 cm^{-1} region. Section 3 includes the rovibronic assignments and the line parameter retrievals together with a pressure dependence study leading to the derivation of the pressure broadening coefficients for a number of lines. Finally, the obtained predissociation rates are discussed in Section 4 in relation with previous experimental and theoretical studies.

2. EXPERIMENT

2.a. The CW-CRDS spectrometer

The CRDS set-up used for the recordings has been described in details in [Kassi2012, Konefał2020, Karlovets2021]. Briefly, the CRDS spectrometer is a 1.4-meter-long high-finesse cavity (HFC) made of a stainless tube fitted with two highly reflective mirrors on its extremities, one of them being mounted on a piezo electric element that allows the cavity length to be slightly length-modulated. Two external cavity diode lasers (ECDL) (DL pro series from Toptica emitting over the 7920-8200 and 8100-8600 cm^{-1} spectral ranges) were used as light source. Their emission frequency was continuously measured by a Fizeau wavemeter (High Finesse WS-U-30 IR, 5 MHz resolution, 20 MHz accuracy). Most of the light intensity is injected into a fibered acousto-optic modulator (AOM) inserted before the HFC which interrupts the excitation once resonance with one of its longitudinal modes is achieved, leading to a ring down (RD) event. Each RD is detected with an InGaAs photodiode. The cavity losses at each laser wavelength were obtained by averaging the results of exponential fits of about tens RD event, thus giving one data point in the spectrum. The absorption coefficient, α (cm^{-1}), was then directly calculated from the decrease of the cavity ring-down time τ (in s) induced by the molecular absorption:

$$\alpha(\nu) = \frac{1}{c}\left(\frac{1}{\tau} - \frac{l}{\tau_0}\right), \quad (1)$$

where c is the light velocity and τ_0 is the ring-down time of the empty cell depending of the mirror transitivity, diffraction losses, volume scattering etc.

An automatic broadband acquisition procedure was implemented to cover the 7920-8100 and 8100-8600 cm^{-1} ranges with the two available ECDLs. It includes, the scan of the ECDL frequency, the selection of mode-hop-free tuning ranges and concatenation of series of slightly overlapping individual 0.8 cm^{-1} spectra (see [Vasilchenko2020, Konefał2020] for details). The sampling step of the recordings was chosen to be about 2×10^{-3} cm^{-1} to be compared to a HWHM Doppler line width of about 7×10^{-3} cm^{-1} (220 MHz) for ozone at 8000 cm^{-1} and an ECDL emission linewidth of 150 kHz at 1 ms integration time. Typically, the recording of a 5 cm^{-1} wide spectral interval required about one hour and about two months were required to cover the whole 7920-8600 cm^{-1} range.

The absolute calibration of the frequency axis as provided by the wavemeter was refined using accurate line centres of O_2 [Konefal2020] or water [Gordon2017], depending on the spectral regions. A final accuracy on the order of 60 MHz (2×10^{-3} cm^{-1}) is estimated for the frequency axis calibration.

2.b. Ozone preparation

A silent electric discharge (12 kV, 400 Hz) at liquid nitrogen temperature (LNT= 77 K) was used to prepare the ozone sample, as described in [Griggs1968]. First, the CRDS stainless steel cell connected to the ozonizer was filled with oxygen (AlphaGaz2 from Air Liquide, purity≥ 99.9995 %) at a typical pressure of P_0= 40 Torr at room temperature (The sample pressure, in the cell, was continuously monitored with a 1000 Torr capacitance gauge). Then the ozonizer was immersed into a Dewar filled with liquid nitrogen (LN) and the discharged was switched on during a few minutes leading to the decrease of the total pressure, the produced ozone being trapped in the ozonizer cooled at LN temperature. After a few minutes, a quasi-complete $3O_2 \rightarrow 2O_3$ conversion was achieved (residual total pressure of about 0.05 Torr), the Dewar was removed and ozone evaporated leading to an initial pressure of pure ozone close to $(2/3)P_0 \approx 26$ Torr.

In spite of our efforts, the slow decomposition of ozone in oxygen was a major issue because of the acquisition time of the spectra. The partial pressure of ozone present in the cell at each time was deduced from the total pressure, $P(t)$, continuously monitored: $P_{O_3}(t) = 2(P_0\text{-}P(t))$. In general, the ozone sample was renewed every 24 hours and during the recording period, the ozone partial pressure was observed to decrease by typically 10 Torr from the 26 Torr initial value. In the following, for the convenience of the data treatment, the obtained absorption coefficients were normalized to an arbitrary constant ozone pressure (*e.g.* 10. Torr). During the various days of the measurement campaign, the temperature was monitored using an analogue temperature sensor (TSic 501, IST-AG, ±0.1 K accuracy) and varied between 293.8 and 294.1 K.

2.c. Overview of the spectrum

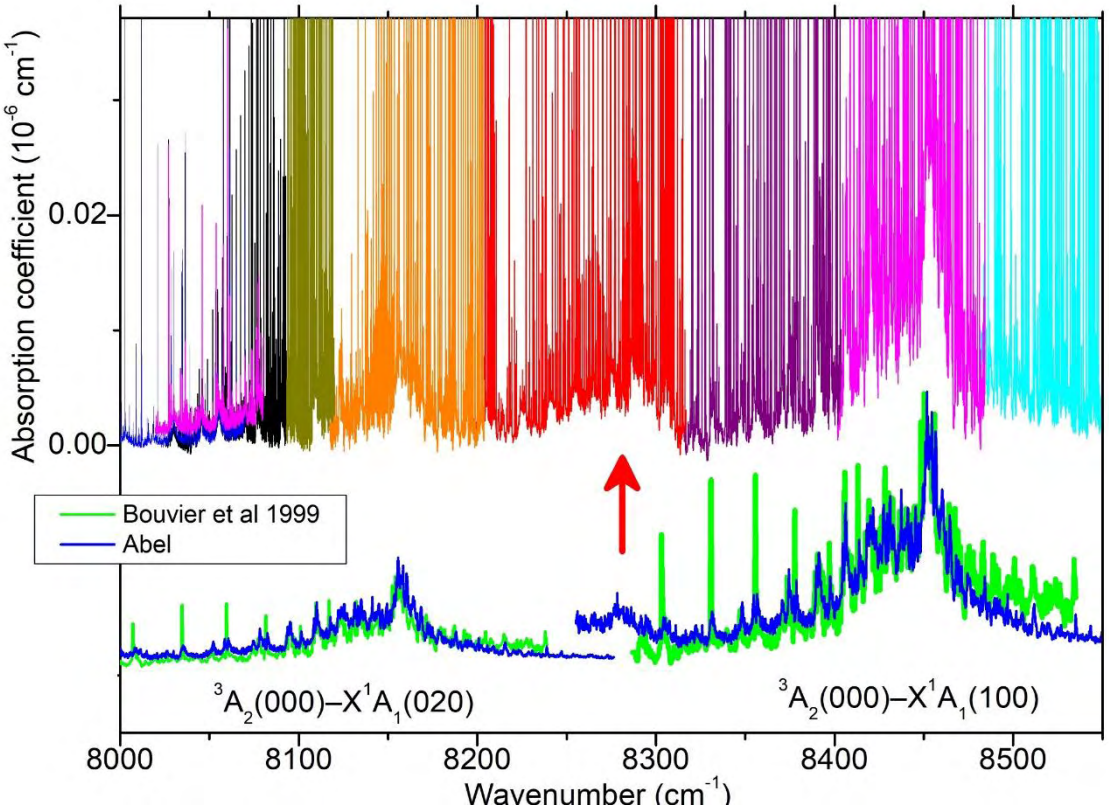

Fig. 2.
Overview of the CRDS ozone recordings between 8000 and 8550 cm^{-1} normalized at the ozone pressure of 10 Torr. The different colours correspond to pieces of spectra recorded with newly generated ozone samples. The spectra are dominated by strong impurity lines (mostly water and CO_2). The ozone absorption shows up as two mostly unresolved bands centred near 8154 and 8450 cm^{-1} due to the $^3A_2(000)$-$X^1A_1(020)$ and $^3A_2(000)$-$X^1A_1(100)$ hot bands, respectively. On the lower part of the figure, the FTS and pulsed-CRDS spectra of the $^3A_2(000)$-$X^1A_1(000)$ cold band observed near 9553 cm^{-1} in [Bouvier1998] and [Wachsmuth2003], respectively, have been shifted in wavenumbers and scaled in intensity to match the two observed hot bands. The arrow near 8285 cm^{-1} points absorption features probably due to the $^3A_2(010)$-$X^1A_1(110)$ hot band.

In order to correct the ozone spectra from cavity loss rate, $1/(c\,\tau_0)$ in Eq. (1), the 7920-8700 cm^{-1} range of the ozone recordings was sampled with recordings over small spectral intervals, with the CRDS cell evacuated. The resulting frequency dependence of the set of $1/(c\,\tau_0)$ loss rates values was obtained from a 4^{th} order polynomial fit *versus* the wavenumber and subtracted from the ozone spectra. The overview of the resulting ozone spectrum in the 8000-8550 cm^{-1} range is presented in **Fig. 2.** In fact, at first glance, ozone absorption is obscured by many strong lines due to impurities: oxygen, water, CO_2 and HF. These species have different origins and their concentration varied during the recordings, depending on the ozone decomposition (in particular, O_2), desorption or chemical reactions with the walls of the setup. Water vapor is most probably desorbing from the gas cell, HF is probably coming from reaction with O-rings and CO_2

might be due to a surface reaction with stainless steel. According to the HITRAN database [Gordon2017], the maximum line intensity values are on the order 5×10^{-26}, 5×10^{-25}, 2×10^{-26} and 3×10^{-20} cm/molecule for oxygen, water, CO_2 and HF, respectively. These values lead to molar fractions of water, CO_2 and HF, on the order of 10^{-3}, 2×10^{-3} and 10^{-5} at most, respectively, and thus to negligible contributions to the total pressure. As discussed above, the partial pressure of oxygen due to the ozone decomposition, can be on the same order as the ozone partial pressure at the end of the spectra recording (see also Fig. 1 of [Vasichenko2020]). This is the reason why, strong O_2 lines are observed in the low energy range of the recordings due to the *R*-branch transitions of the $a\ ^1\Delta_g(0) - X\ ^3\Sigma_g^-(0)$ band centered near 7884 cm^{-1}.

At the scale of the overview of **Fig. 2**, the ozone absorption signature shows up as two partly unresolved and broad absorption bands which form the baseline where are superimposed the narrow lines due to impurities. These two bands with maximum near 8154 and 8450 cm^{-1} are hot bands from the (020) and (100) ground state vibrational levels reaching the same predissociated $^3A_2(000)$ state of $^{16}O_3$ (see **Fig. 1**). This is confirmed by comparison to the FTS and pulsed-CRDS spectra of the $^3A_2(000)$-$X^1A_1(000)$ cold band centered near 9553 cm^{-1} recorded in [Bouvier1998] and [Wachsmuth2003], respectively. The wavenumber scale of the cold band spectra included in **Fig. 2** has been shifted by the (020) and (100) vibrational term (1399 and 1103 cm^{-1}, respectively). The shifted cold band spectra (scaled in intensity to match the CRDS envelopes) show a strong similarity to the CRDS baseline envelopes which will be confirmed below by a detailed examination of the narrow absorption lines at high resolution. Let us mention that an additional broad absorption structure is observed near 8285 cm^{-1} in coincidence to the expected center of the $^3A_2(010)$-$X^1A_1(110)$ band (8286 cm^{-1} according to **Fig. 1**).

3. SPECTRA ANALYSIS

3.a. Rovibrational assignments

In order to illustrate the appearance of the CRDS spectrum at high resolution, **Fig. 3 (a)** and **(b)** presents expanded views in two narrow spectral intervals. In the region around 8123 cm^{-1}, absorption features with a large variety of widths are observed. Most of them are unassigned ozone lines. Some lines have a small "standard" width, similar to that of impurity lines of CO_2 or water which appear superimposed. Other ones are much broader due to predissociation. The superposition of broadened absorption lines leads to a continuum background mostly structureless. Among the highly congested absorption features, appear a few regular sequences of narrow lines as that presented in **Fig. 3 (b)** around 8394 cm^{-1} (The displayed sequence of lines, with similar width, are among the set of narrow lines which could be assigned using previous spectroscopic studies of the $^3A_2(000)$-$X^1A_1(000)$ cold band centered near 9550 cm^{-1} (see **Fig. 3 (c)** and below).

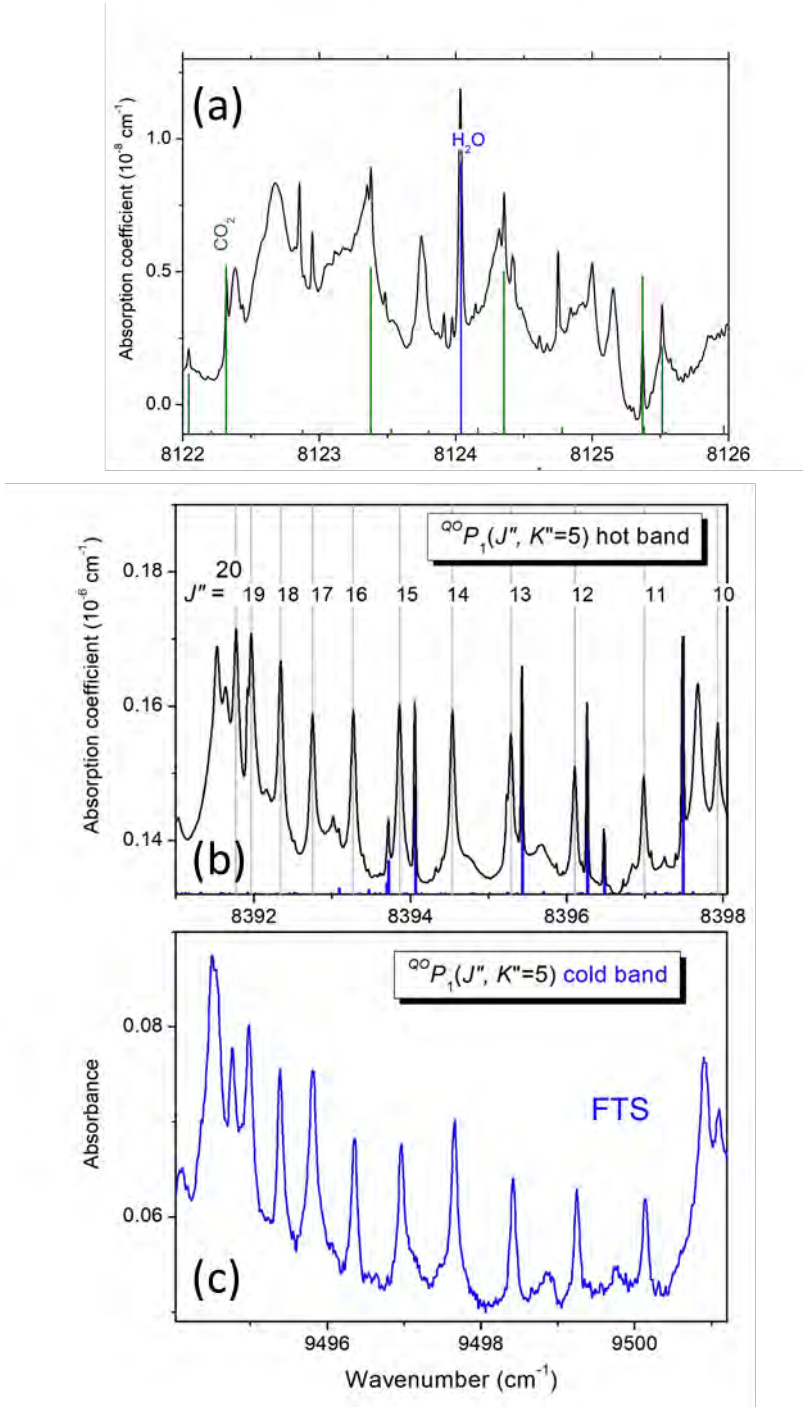

Fig. 3. Samples of ozone spectra

(a) CRDS spectrum near 8123 cm^{-1} showing a variety of lines broadened by predissociation. A number of narrow lines, due to CO_2 and water present as impurities, are identified by comparison with the corresponding HITRAN stick spectra (green and blue, respectively),

(b) CRDS spectrum near 8394 cm^{-1} showing the $^{QO}P_1(K''= 5, J'')$ series of the $^3A_2(000)$-$X^1A_1(100)$ hot band. The lines of this series show limited predissociation widths, all with similar magnitude,

(c) FTS spectrum near 9498 cm^{-1} corresponding to the same $^{QO}P_1(K''= 5, J'')$ series in the $^3A_2(000)$-$X^1A_1(000)$ cold band. The displayed spectrum was recorded in [Bouvier1998] (T= -51.58°C, P= 20 Torr, L=100 meters).

In the following, we will focus on the line profile study of relatively narrow lines with rotational assignment. In [Bouvier1998], about one hundred lines of the cold band are reported with assignments from the FTS spectrum between 9100 and 9550 cm^{-1} (see this reference for the definition of the quantum numbers and the notation of the different branches).

It is straightforward to transfer the (*J', K'*)← (*J'', K''*) rotational assignment of a cold band transition assigned in [Bouvier1998] to the hot band transitions from the (100) and (020) lower states. The energy of the (*J', K'*) upper level is obtained by adding the energy of the (*J'', K''*) ground state level to Bouvier's wavenumber. The wavenumber of the corresponding hot band transitions is obtained by the difference between the determined (*J', K'*) upper energy and the energy value of the (*J'', K''*) level of the (100) [or (020)] lower states. The FTS line centres are given in [Bouvier1998] with a typical accuracy on the order of 10^{-2} cm^{-1}. The rovibrational energies of the X^1A_1 (000), (100) and (020) levels are known with a high accuracy (better than 10^{-3} cm^{-1}) and collected, for instance, in the web-accessible information system "Spectroscopy & Molecular Properties of Ozone" (SMPO) [Babikov2014] (http://smpo.iao.ru; http://smpo.univ-reims.fr). The matching (within typically 0.01 cm^{-1}) of the obtained line centers with positions of narrow lines observed in our spectrum allowed to unambiguously assign about 50 and 30 lines of the hot band from (100) and (020), respectively. The line widths being (partly) ruled by the predissociation rate of the upper state, corresponding lines show similar line profile in the cold and hot bands. In particular, the regular sequences assigned in the cold band have very similar appearance in their hot band counterparts as illustrated by the direct comparison of the present CRDS spectrum and the FTS spectrum reported in [Bouvier1998] of the ${}^{QO}P_1(K''= 5, J'')$ series in the hot and cold band, respectively (**Fig. 3b and 3c,** respectively).

3.b. Line parameter retrieval

All the previous line profile analyses were performed on spectra recorded at lower spectral resolution. The best resolved spectra of the cold band were obtained by ICLAS [Abel1997] and FTS in [Bouvier1998], [Inard1998]) with a spectral resolution of 0.014 cm^{-1} and 0.02 cm^{-1}, respectively, on the same order of magnitude than the Doppler broadening (about 0.015 cm^{-1} or 440 MHz, FWHM). In this work, the emission width of our laser sources is much smaller than the Doppler broadening, so that the contribution of the apparatus function to the observed profiles is negligible allowing improvement of the accuracy on the fitted parameters and particularly on the predissociation rates.

The line parameters were retrieved by using a homemade interactive least squares multi-lines fitting program written in LabVIEW. The fits were performed over narrow spectral intervals which could be fitted independently and include ozone lines and overlapping impurity lines (water and CO_2). The Gaussian width was fixed to the Doppler broadening calculated according to the mass of the species and the measured temperature of the gas. For each spectral interval, the line center (ν_0), integrated absorption coefficient (A_{ν_0}

in cm^{-2}/molecule) and Lorentzian width of each line as well as the baseline (assumed to be a linear function of the wavenumber) were fitted. Note that the fitted Lorentzian width, Γ_P, results from the sum of the broadening effects due to pressure and predissociation. The intensity, $S_{\nu_0}(T)$ of a line centered at ν_0 was calculated from the integrated absorption coefficient:

$$A_{\nu_0} = \int_{line} \alpha_\nu \, d\nu = S_{\nu_0}(T)N \qquad (2)$$

Where α_ν is the absorption coefficient in cm^{-1} obtained from the cavity ring down time (Eq. 1) and N is the volume number density in molecule/cm^3 obtained from the measured pressure and temperature values: $N = P/k_BT$ with k_B the Boltzmann constant.

The line parameter derivation was made difficult by the considerable spectral congestion. As illustrated in **Fig. 4** in the case of the $^{QQ}Q_2(9, J)$ progression, the large broadening of some ozone lines made difficult to determine the baseline and results in larger error bars on the largest widths.

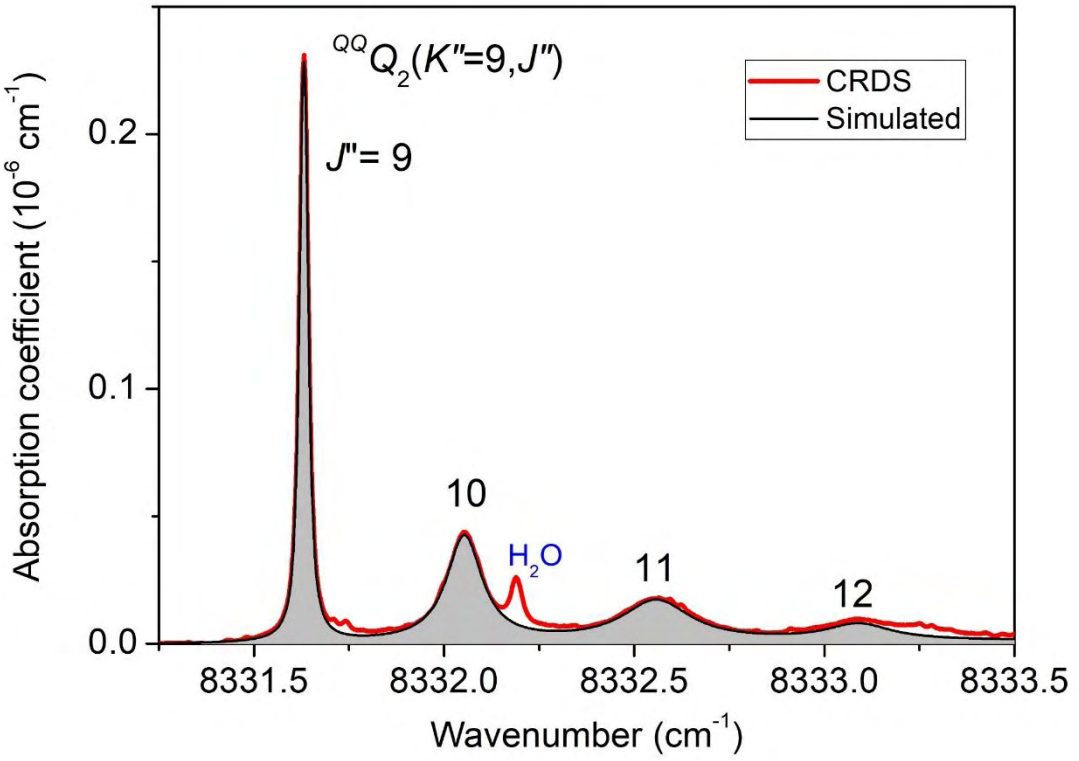

Fig. 4.
Line parameter retrieval for the $^{QQ}Q_2(9, J'')$ progression of the $^3A_2(000)$-$X^1A_1(100)$ hot band of $^{16}O_3$ recorded by CRDS (red). The fit of the spectrum included minor absorption features (including the indicated water line near 8332.19 cm^{-1}) but the simulation (black solid line) is limited to the four assigned $^{QQ}Q_2(9, J'')$ lines. Note the rapid increase of the predissociation width with increasing J'' values.

The obtained list of line parameters is provided as Supplementary Material. Together with ν_0, $S_{\nu_0}(T)$ and Γ_P, the line list includes the lower state energy, E'', as provided by SMPO [Babikov2014] and the value

of the upper state energy (*E'*) derived from our transition wavenumber. Note that the two hot bands and the cold band measured by FTS [Bouvier1998] provide several energy determinations of the same upper level which can be compared. A given upper level can be reached *(i)* from the (020), (100) and ground vibrational states through transitions with identical rotational assignment and *(ii)* through transitions of the same hot or cold band, belonging to different branches. The comparison of the *E'* values shows the good consistency between the CRDS values derived from the two hot bands with a general agreement within 6×10^{-3} cm^{-1}. This agreement is satisfactory considering the uncertainty on the line center determination in the case of lines broadened by predissociation. On average, the *E'* values derived from the FTS line positions of the cold band [Bouvier1998] agree with our values but are systematically smaller by about 0.01 cm^{-1}, probably due to a calibration shift of the FTS spectra by the same amount. Note that, in the same way as for *E'*, when a given upper energy level can be reached through different transitions, different determinations of the predissociation rate of the upper level are obtained independently from the line widths. The comparison of the various determinations will be presented below after an evaluation of the pressure broadening contribution to the Lorentzian width presented in the following line profile analysis.

3.c. Pressure broadening

Twenty years ago, the "metastability" of the $^3A_2$ electronic state was a subject of discussion between Bouvier et al. [Bouvier1998, Bouvier1999] and Abel et al. [Abel1997, Wachsmuth2003]. These two groups dedicated efforts to the measurements of the upper state life time from the measured line widths in the $^3A_2(000)$-$X^1A_1(000)$ cold band. In particular, Bouvier et al. pointed the existence of narrow lines with very small predissociation broadening as a potential confirmation of the "metastability" of the $^3A_2$ electronic state predicted by *ab initio* calculations [Minaev1994, Braunstein1995]. In fact, the spectral resolution of the spectra analyzed by these two groups was insufficient to access the predissociation width of the narrowest lines. Bouvier et al. analysis relied on FTS spectra while Abel et al. recorded spectra by ICLAS and pulsed CRDS. None of the used setup has a Doppler limited resolution (the best claimed spectral resolution of 0.014 cm^{-1}, by ICLAS [Abel1997] is about twice the Doppler broadening). In addition, the predissociation broadening, Γ_0, must be deduced through extrapolation to zero pressure of the Lorentzian width which requires the determination of the self-broadening coefficient. The only study of the pressure dependence of broadening of the narrow lines was performed by pulsed CRDS with a spectral resolution limited to 0.03 cm^{-1} [Wachsmuth2003]. In addition to the insufficient spectral resolution, the use of a pulsed CRDS setup led to multi-exponential decay of the cavity modes and to the introduction of corrector factors which affected the line profile [Wachsmuth2003]. As a result, very large broadening coefficients were reported for the studied cold band transitions, in strong disagreement with our results (see below).

The experimental contribution to the line profile being negligible in continuous-wave CRDS, we performed a series of measurements to clarify if some of the narrowest lines have their zero-pressure width

limited by Doppler broadening i.e. mostly free of predissociation broadening. Eighteen narrow lines listed in **Table 1** were selected for a pressure dependence study. First, the cell was filled with ozone at 40 Torr and the spectrum was recorded over a small spectral interval around the targeted line, following the method described above for the extensive recordings. Then part of the gas was evacuated to decrease the pressure successively to 30, 20 and Torr and a new spectrum was recorded for each pressure value. About three hours were needed for the series of recordings. Taking into account ozone the ozone dissociation rate of 0.23 Torr/h uncertainty, a maximum error of 7% is estimated or lowest pressure value. Note that the recording of spectra over narrow spectral intervals just after the ozone generation led to smaller contribution of the lines due to impurities compared to the broad range recordings presented in **Fig. 2.**

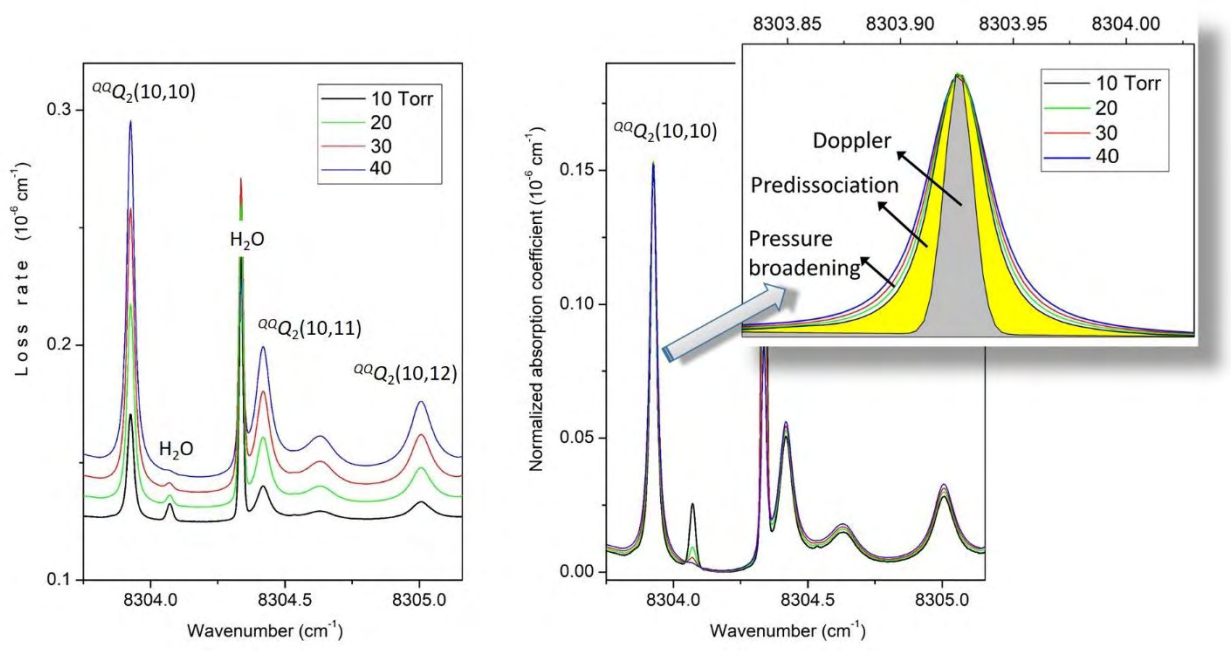

Fig. 5.

Pressure dependence of the absorption spectrum in the region of the $^{QQ}Q_2(10, J")$ progression of the $^3A_2(000)$-$X^1A_1(100)$ hot band of $^{16}O_3$.

Left panel: Variation of the loss rate of the CRDS cavity for pressure values between 10 and 40 Torr. Note the important variation of the baseline increasing linearly with pressure,

Right panel: Same spectra corrected from the baseline and scaled (according to the 40 Torr spectrum) to show the small width increase due to pressure broadening. The insert shows an enlarged view of the $^{QQ}Q_2(10,10)$ line. The inset shows a zoom of the $^{QQ}Q_2(10,10)$ line with a simulation of the Doppler profile. The pressure and predissociation contributions to the measured width are highlighted.

The variation of the spectrum with pressure values between 10 and 40 Torr is illustrated in **Fig. 5** for the $^{QQ}Q_2(10,J"=10\text{-}12)$ lines of the $^3A_2(000) \leftarrow X^1A_1(100)$ hot band. On the left hand panel, the raw spectra are presented as measured cavity loss rates, without baseline correction. On the right hand panel, the baseline has been approximately corrected and the spectra are normalized by the pressure. The inset shows an

expanded view of the $^{QQ}Q_2(10,10)$ line which is one of the narrowest lines. The high signal-to-noise ratio of the spectra allows evidencing the extra pressure broadening which is clearly visible but remains small compared to the overall line width. A simulation of the Doppler line profile has been added to illustrate the fact that the line is affected by an extra broadening due to predissociation.

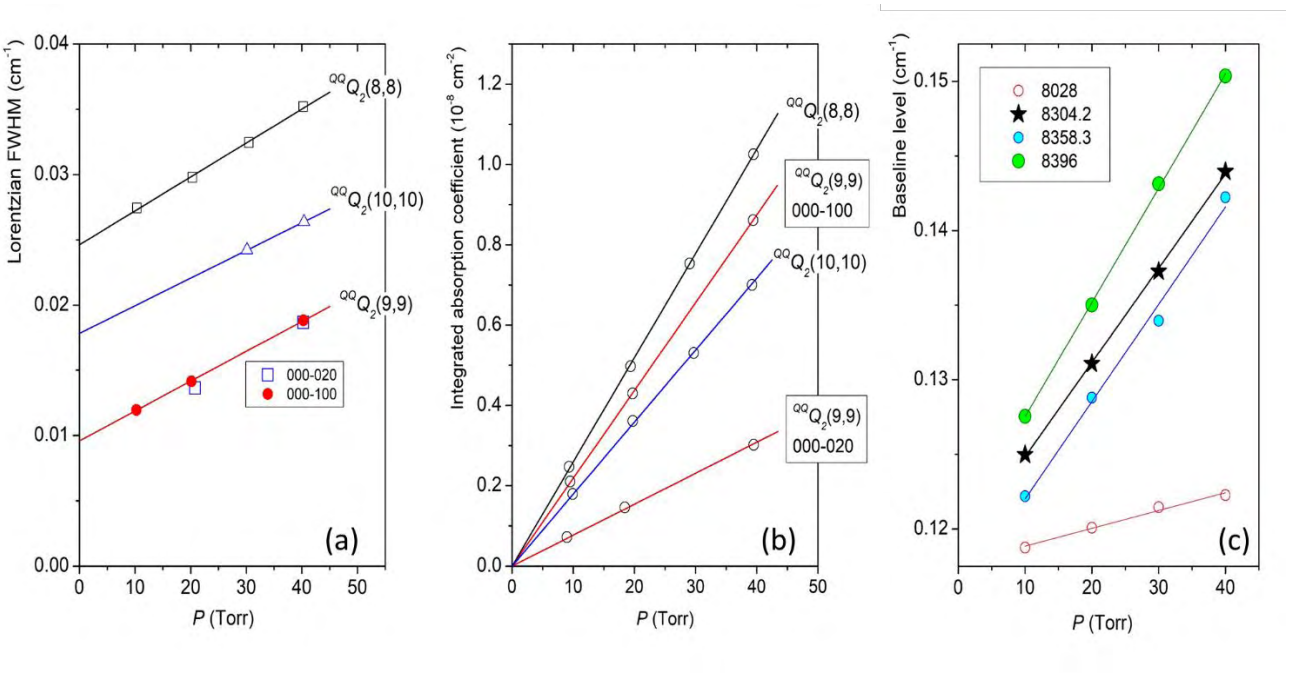

Fig. 6.
Pressure dependence of Lorentzian width *(a)*, integrated absorption coefficient *(b)* and baseline level *(c)*.
The same four narrow lines are considered in *(a)* and *(b)*. Note that they include two $^{QQ}Q_2(9,9)$ lines reaching the same $^3A_2(000)$ upper level from (020) and (100) ground state vibrational levels.
The pressure dependence of the baseline level is plotted in *(c)* at four spectral points free of narrow absorption lines.

This is confirmed by the pressure dependence of the Lorentzian widths displayed on **Fig. 6 (a)**. (The line parameter retrieval was performed in the same way as described above, independently for each pressure value). The pressure broadening coefficients, included in **Table 1,** were obtained from the slope of a linear fit of the Lorentzian widths *versus* pressure. Note that the width due to predissociation corresponds to the Lorentzian FWHM at null pressure on this graph. In the same way, line intensities were obtained from the proportionality factor of the integrated absorption coefficient and pressure (see **Fig. 6 (b)** and Eq. 2). As mentioned above, the two hot bands may give access to the same upper level. We have included on **Fig. 6 (a)**, the pressure dependence of the Lorentzian width of the $^{QQ}Q_2(9,9)$ line measured from the (020) and (100) lower levels. As expected, the widths obtained from the two transitions are found in close coincidence.

Table 1.
Line parameters of the eighteen ozone lines used for the pressure dependence study.

Transition $^{\Delta K \Delta N}\Delta J_{Fi}(K,J)$	Lower vibrational level	Position (cm^{-1})	Line intensity (10^{-27} cm/molecule)	γ_{self} *(FWHM)* (cm^{-1}/atm)	Γ_0 *(FWHM)* (10^{-2} cm^{-1})
$^{QQ}Q_{F2}(9,9)$	020	8027.2090	2.347(29)	0.186(10)	0.86(4)
$^{QQ}Q_{F2}(10,10)$	100	8303.9257	5.459(28)	0.161(2)	1.78(1)
$^{QQ}Q_{F2}(10,11)$	100	8304.4186	3.963(54)	0.228(19)	4.800(7)
$^{QQ}Q_{F2}(10,12)$	100	8305.0062	3.234(32)	0.241(83)	8.13(34)
$^{QQ}Q_{F2}(9,9)$	100	8331.6317	6.657(13)	0.174(2)	0.96(1)
$^{QQ}Q_{F2}(8,8)$	100	8356.5153	7.901(26)	0.197(5)	2.46(2)
$^{QQ}Q_{F2}(8,9)$	100	8356.9137	4.94(17)	0.463(239)	7.63(87)
$^{QQ}Q_{F2}(8,10)$	100	8357.428	3.83(18)	0.58(28)	14.9(10)
$^{QQ}Q_{F2}(8,11)$	100	8358.014	2.164(61)	0.81(13)	18.55(53)
$^{QO}P_{F1}(5,20)$	100	8391.7710	6.755(15)	0.324(58)	8.19(21)
$^{QO}P_{F1}(5,19)$	100	8391.9650	4.72(10)	0.205(89)	6.50(33)
$^{QO}P_{F1}(5,18)$	100	8392.3420	5.62(17)	0.110(130)	7.23(48)
$^{QO}P_{F1}(5,17)$	100	8392.7483	4.686(44)	0.130(26)	7.69(10)
$^{QO}P_{F1}(5,16)$	100	8393.2697	4.627(50)	0.162(65)	6.94(24)
$^{QO}P_{F1}(5,15)$	100	8393.8619	5.34(13)	0.391(10)	6.36(4)
$^{QO}P_{F1}(5,14)$	100	8394.5378	4.342(30)	0.205(26)	6.41(9)
$^{QO}P_{F1}(5,13)$	100	8395.2868	4.025(43)	0.227(36)	6.39(13)
$^{QO}P_{F1}(5,12)$	100	8396.1026	3.34(23)	0.142(62)	6.23(23)

Finally, on **Fig. 6 (c)**, the pressure dependence of the baseline level is presented for four spectral points located in different regions "free" of absorption lines. In particular, the 8304.2 cm^{-1} spectral point illustrates the variation of the base line level presented in **Fig. 5 (a).** For the four chosen wavenumber values, the baseline level is found to increase linearly with pressure, indicating that a large part of the total absorption of the considered hot bands is due to an unresolved "continuum" resulting from the superposition of broad predissociated lines.

In **Fig. 7 (a)**, the broadening coefficients, γ_P (FWHM in cm^{-1}/atm) of the studied transitions are plotted *versus* the upper state rotational number, *J'*. The zero-pressure value of the Lorentzian widths, Γ_0 in cm^{-1}, provided by the linear fit corresponds to the predissociation broadening (**Fig. 7 (b)**). If we exclude, the three broad $^{QQ}Q_2(8,\ J''= 9\text{-}11)$ lines for which the large predissociation broadening prevents an accurate determination of the pressure broadening, most of the γ_P values are around 0.20 cm^{-1}/atm. This value is close to the default value of 0.18 cm^{-1}/atm (FWHM) recommended by the HITRAN database for the rovibrational transitions [Gordon2017]. We have included in **Fig. 7 (a)** (full grey circles), the self-broadening coefficients calculated according to the empirical law proposed in [Starikov2011] on the basis of measurements of the pure rotational band and of the ν_2 infrared band. This law includes a small dependence according to the rotational quantum numbers. If we except the $^{QO}P_1(5,15)$ unexplained outlier, our measurements show an overall agreement with the empirical law of [Starikov2011] indicating that, within our experimental uncertainties, this empirical law is valid for the considered electronic transitions. As mentioned above, this

result contradicts the pulsed CRDS measurements in the cold band who stated “the pressure broadening coefficient for ozone self-collisions (for excitation in the triplet state) is an order of magnitude larger than for self-collisions of ozone in vibrationally excited states of the ground electronic state” [Wachsmuth2003].

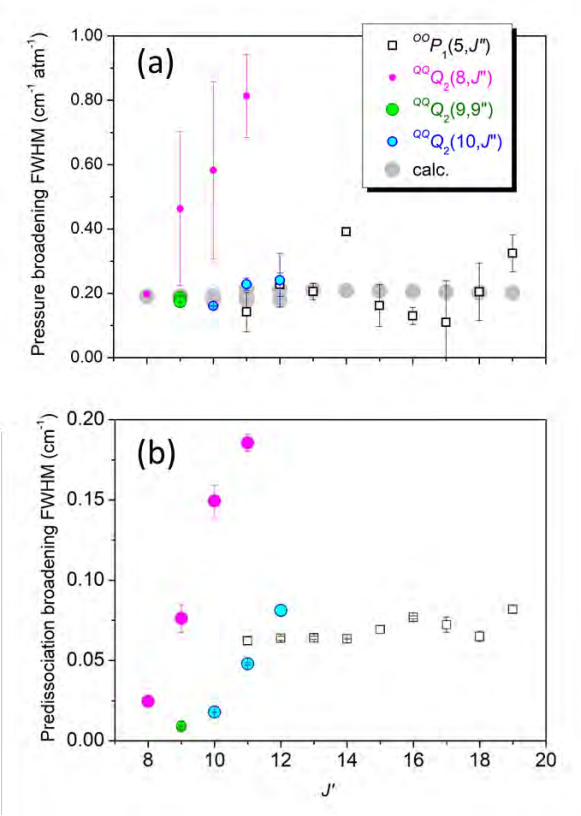

Fig. 7.
Variation of the pressure broadening coefficient (FWHM, cm^{-1}/atm) and of the predissociation width (FWHM, cm^{-1}) *versus* the upper *J* value of the transitions listed in **Table 1**. The experimental values for four series of transitions are plotted with different color. The self-broadening coefficients calculated according to the empirical law proposed in [Starikov2011] for rovibrational transitions are plotted on the upper panel (full grey circles),

In order to obtain the predissociation broadening of the about 40 remaining lines retrieved at a single pressure (of about 25 Torr), the fitted values of their Lorentzian widths were decreased by the pressure broadening contribution, calculated using the empirical law recommended in [Starikov2011].

3.d. Predissociation broadening

In the Supplementary Material, the listed predissociation broadenings values are thus obtained from the pressure dependence study for 18 lines or empirically corrected from the pressure broadening for 40 lines. The overall set of Γ_0 values are plotted in **Fig. 8** *versus* the upper level energy. The Γ_0 values range between about 0.01 and 0.3 cm^{-1}.

For a number of $^3A_2(000)$ upper levels, we have at disposal two or three determinations of Γ_0 (and *E'*) obtained from different transitions (either within the same band or from the two hot bands). The

consistency of the various determinations is in general very satisfactory as seen for instance in the insert of **Fig. 8** [red circles and green crosses correspond to hot band transitions from the (100) and (020) vibrational levels, respectively. Double red symbols correspond to transitions from two branches of the hot band from (100)].

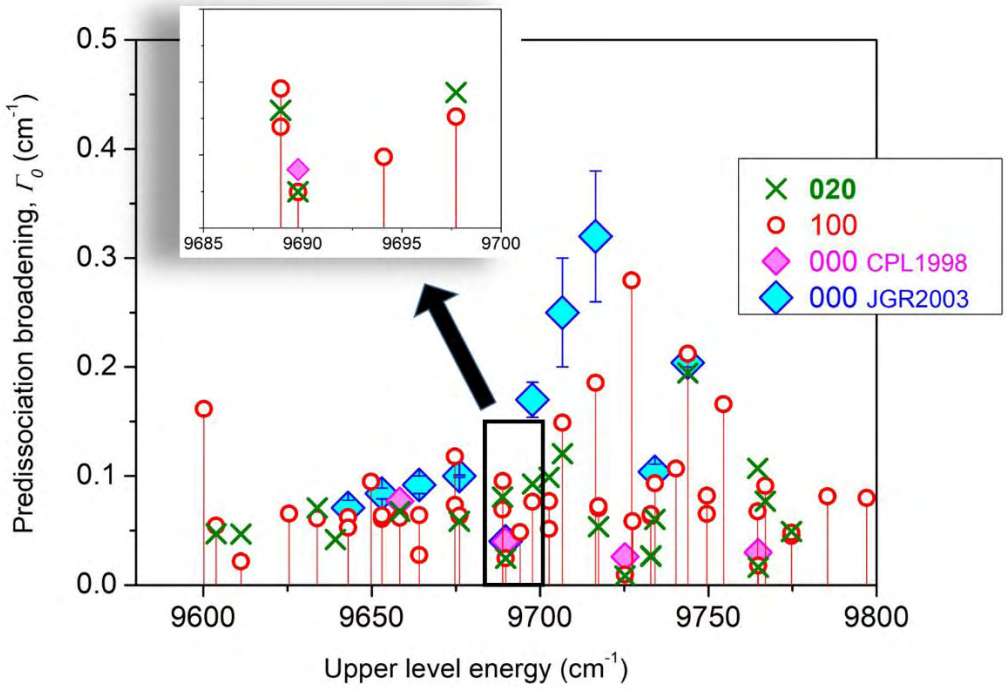

Fig. 8.
Variation of the predissociation width (FWHM, cm^{-1}) *versus* the upper energy value of the transitions provided as Supplementary Material. Green crosses and red open circles correspond to the $^3A_2(000)$-$X^1A_1(020)$ and $^3A_2(000)$-$X^1A_1(100)$ hot band transitions, respectively. Values obtained by Inard et al. [Inard1998] and Wachsmuth&Abel [Wachsmuth2003] on the basis of FTS and pulsed-CRDS spectra in the $^3A_2(000)$-$X^1A_1(000)$ cold band are also plotted (pink and blue diamonds, respectively).
The inset illustrates the agreement in the case of various determinations of the predissociation rate of the same upper level excited through different transitions.

As first noted in [Bouvier1998] and [Wachsmuth2003], in a number of well resolved *K* sub-bands, the first line, $^{QQ}Q_2(K'', J''= K'')$, corresponds to the smallest predissociation broadening (see K''= 8-10 in **Fig. 7 (b)**). Our measurements allowed for measuring accurately the small corresponding Γ_0 values while previous measurements were inconclusive due to the lack of spectral resolution and the insufficient knowledge of pressure broadening effects. The $^{QQ}Q_2(8,8)$ line which has the smallest width could be measured from the (020) and (100) lower states (**Table 1**). The Γ_0 values provided by the multispectrum treatment are $8.6(4)\times10^{-3}$ and $9.6(1)\times10^{-3}$ cm^{-1} (FWHM), respectively. Considering that these values correspond to about half of the Doppler broadening (see also inset in **Fig. 5**), the achieved agreement is

satisfactory. In conclusion, although small, the predissociation broadening of the narrowest lines has been reliably determined and we could not identify any line free of predissociation effects.

The dissociation widths previously determined from the $^3A_2(000) \leftarrow X^1A_1(000)$ cold band are included in **Fig. 8** for comparison. Inard et al. focused on the narrowest lines and reported Γ_0 values for four $^{QQ}Q_2(K'', J''= K'')$ transitions with K''= 7-11 [Inard1998]. The measurements were particularly challenging because the resolution of their FTS spectra was similar or even larger of the Γ_0 values to be measured. Inard et al. reported only an average value with large error bar, Γ_0= 0.035±0.04 cm^{-1}, for the four lines $^{QQ}Q_2(K'', J''= K'')$, with K''= 7-11. Although systematically larger (see **Fig. 8)**, the FTS results are in reasonable agreement with our values, except for the very narrow above mentioned $^{QQ}Q_2(8,8)$ line for which our two determinations are smaller by a factor of about 3.

In total, Wachsmuth and Abel reported eleven Γ_0 values belonging to the $^{QQ}P_1(5, J'')$, $^{QQ}Q_2(8, J'')$ and $^{QQ}Q_2(9, J'')$ series of the cold band [Wachsmuth2003]. Their values relied on a pressure dependence study but suffered some experimental limitations. The maximum spectral resolution of their CRDS setup was 0.03 cm^{-1} and non-exponential decay of the ring down intensity had to be corrected. As a result, self-broadening coefficients on the order of 1 cm^{-1}/atm were reported. These values are considerably larger than both our measurements relative to the two hot bands and to the values obtained from vibrational bands (about 0.18 cm^{-1}/atm FWHM [Starikov2011]). Nevertheless, the resulting pulsed CRDS Γ_0 values included in **Fig. 8**, show an overall good agreement with our results, except for three wide lines for which the pulsed CRDS values are significantly larger than ours (probably due to the difficulty of properly estimating the baseline in the case of wide absorption features).

4. Discussion-Predissociation mechanism

The $^3A_2$ electronic state of ozone is the lowest of the three triplet states at the origin of the Wulf band [Minaev1994, Braustein1995, Anderson1995, Grebenshchikov2007]. The global potential energy surfaces (PES) of the $^3A_2$, $^3B_2$ and $^3B_1$ states have been calculated [Grebenshchikov2007]. The $^3A_2$ PES has a local minimum around 9500 cm^{-1} which is above the dissociation threshold corresponding to the $O(^3P) + O_2(\tilde{X}\ ^3\Sigma_g^-)$ channel at about 8560 cm^{-1} [Ruscic2010, Holka2010]. This $^3A_2$ PES is one of the 27 PESs converging to this limit including the one of the ground electronic state [Rosmus2002].

Grebenshchikov et al. [Grebenshchikov2007] and Xie et al. [Xie2001] have evaluated theoretically the predissociation rate of the $^3A_2(000)$ state from tunneling effect through the barrier of the $^3A_2$ PES and obtained Γ_0 values of 8 and 9×10^{-4} cm^{-1}, respectively. This value is 10 times smaller than our minimum value of 0.009 cm^{-1} measured for the predissociation broadening of the $^{QQ}Q_2(8,8)$ transition.

In agreement with Bouvier et al. [Bouvier1998], Grebenshchikov et al. [Grebenshchikov2007] concluded that the large measured predissociation rates are enhanced by a spin-orbit (S-O) coupling

inducing a singlet-triplet mixing of $^3A_2(000)$ with some highly excited dissociative vibrational states of the X^1A_1 ground state. A tiny part (~1%) of the dissociative character of the X^1A_1 vibrational levels is then transferred to the $^3A_2(000)$ level, drastically decreasing the upper state lifetime.

As a result, the rates of predissociation *via* the S-O interaction vary strongly with the upper states according to their *J* and *K* rotational quantum numbers and the energy gap between the coupled pair of rotational levels of the $^3A_2(000)$ and $X^1A_1(v_1,v_2,v_3)$ states. This is reflected by the variety of Γ_0 values presented in **Fig. 8**. Let us remind that this figure is limited to relatively narrow lines. Large Γ_0 values are difficult to determine experimentally and are thus absent from this plot.

In [Mondelain2012], some theoretical insights were presented to explain the variation of the predissociation broadening of the $^{QQ}Q_2(K'', J''= K'')$ lines of the $^{18}O_3$ isotopologue. The spectroscopic information relative to the $^3A_2(000)$ state of $^{18}O_3$ were retrieved from a CRDS spectrum recorded between 7600 and 7920 cm^{-1} where transitions belonging to the $^3A_2(000)$-$X^1A_1(110)$ hot band could be assigned. The predissociation rate of the upper state of the $^{QQ}Q_2(K'', J''= K'')$ transitions were found to exhibit two strong local increases for K''= 3-4 and K''= 10. These increased predissociation rates are due to an energy crossing with highly excited X^1A_1 vibrational states ("doorway states"). Theoretical calculations were performed to identify the high lying doorway states of X^1A_1 involved in the S-O interaction with the $^3A_2(000)$ state of $^{18}O_3$. Accurate predictions of X^1A_1 involved resonance states are particularly demanding in the energy region of the $^3A_2(000)$ state which is about 1000 cm^{-1} higher than the dissociation energy, D_0. From the series of rovibrational energies predicted using an empirical potential function [Tyuterev2000] of the X^1A_1 electronic ground state and their vibrational overlap with the $^3A_2(000)$ state, a few of X^1A_1 vibrational levels above the dissociation threshold [of $(v_1\, v_2\, v_3=0)$ type] were tentatively identified as responsible for the predissociation of the considered states of $^3A_2(000)$. Following the same approach, the predissociative mechanism of the same series of upper states of $^{QQ}Q_2(K'', J''= K'')$ transitions in the main isotopologue, $^{16}O_3$, was found to be similar although more complex as it involves a higher number of candidates for the ''doorway'' states [Mondelain2012]. As concerns the strong linewidth increase with *J* observed in the $^{QQ}Q_2(K'', J'')$ progression for a given K'' value (see *e.g.* **Fig. 4)**, it was qualitatively interpreted as mainly due to the *J* dependence of the singlet-triplet coupling matrix elements.

In the present work, we did not attempt to interpret the rotational dependence of the extended set of measured predissociation rates. This future work will benefit of recent improvements of the ozone PES. The lifetimes of the X^1A_1 metastable states above the dissociation threshold have been evaluated for J= 0,1 in [Lapierre2016] using the *ab initio* PES of [Tyuterev2000]. Further theoretical work will be necessary to extend this study the higher *J* values and to determine the transition probabilities between rovibrational states of the X^1A_1 and $^3A_2$ states due to the S-O coupling.

5. CONCLUSION

The very weak absorption spectrum of ozone in the low energy tail of the Wulf band has been measured for the first time in the 7920-8700 cm^{-1} range. The spectrum includes two newly observed electronic hot bands with maximum near 8154 and 8450 cm^{-1}. The corresponding transitions reach the same predissociated $^3A_2(000)$ upper state from the (020) and (100) ground state vibrational levels. Absorption line profiles are affected by an extra Lorentzian broadening due to the predissociation of the $^3A_2(000)$ upper state. The Doppler resolution of the present CRDS recordings allowed for a detailed line profile analysis. The pressure broadening coefficients of 18 lines, among the narrowest, were accurately determined from the analysis of a series of recordings performed at different pressures. The pressure and predissociation contributions to the line profile could be disentangled. As a result, the pressure broadening of the two studied hot bands is found to be similar to that of the vibrational bands and none of the studied lines is free of predissociation effects. The smallest predissociation width is about 10^{-2} cm^{-1} and corresponds to an upper state life time of about 500 ps. This is about ten times shortest than the life time from tunneling effect through the barrier of the $^3A_2$ PES evaluated theoretically in [Grebenshchikov2007] and [Xie2001], confirming the importance of the spin-orbit coupling mechanism of $^3A_2(000)$ with some highly excited dissociative vibrational states of the X^1A_1 ground state. The set of accurate life times determined from sixty lines will be valuable to identify the ground state doorway states responsible of the predissociation.

Further work is still required to complete the analysis of the recorded CRDS spectra. Indeed, in addition to the two studied hot bands, two additional hot bands are expected to contribute to the high energy part of the recorded spectra: according to **Fig. 1**, the excitation of the $^3A_2(000)$ level from the (010) ground state level leads to a hot band with a maximum near 8852 m^{-1} while the hot band from (020) to $^3A_2(010)$ is predicted around 8684 cm^{-1}. The narrow lines being located in the low energy side of the bands, predissociated lines are expected to be present in the range of our recordings (up to 8700 cm^{-1}). Note that the $^3A_2(010)$-$X^1A_1(000)$ cold band has been studied by FTS [Bouvier2001] and similar predissociation effects affect the $^3A_2(010)$ and the $^3A_2(000)$ states. The spectral resolution of our spectra will allow improved characterization of these effects in $^3A_2(010)$.

Acknowledgements

This work was supported by the Russian Science Foundation Grant No. 19-12-00171 and by CNRS (France) in the frame of the International Research Project “SAMIA” with IAO-Tomsk.

References

[Abel1997]
Abel, Bernd, Aleš Charvát, and Sabine F. Deppe. 1997. "Lifetimes of the Lowest Triplet State of Ozone by Intracavity Laser Absorption Spectroscopy." Chemical Physics Letters 277(4):347–55. doi: 10.1016/S0009-2614(97)00893-2.

[Anderson1985]
Anderson, S. M., F. S. Klein, and F. Kaufman. 1985. "Kinetics of the Isotope Exchange Reaction of 18O with NO and O2 at 298 K." The Journal of Chemical Physics 83(4):1648–56. doi: 10.1063/1.449402.

[Anderson1995]
Anderson, S. M., and K. Mauersberger. 1995. "Ozone Absorption Spectroscopy in Search of Low-Lying Electronic States." Journal of Geophysical Research 100(D2):3033. doi: 10.1029/94JD03003.

[Babikov2014]
Babikov, Yurii L., Semen N. Mikhailenko, Alain Barbe, and Vladimir G. Tyuterev. 2014. "S&MPO - An Information System for Ozone Spectroscopy on the WEB." Journal of Quantitative Spectroscopy and Radiative Transfer 145:169–96. doi: 10.1016/j.jqsrt.2014.04.024.

[De Backer-Barilli2006]
De Backer-Barilly, M. R., A. Barbe, Vl G. Tyuterev, D. Romanini, B. Moeskops, and A. Campargue. 2006. "Fourier Transform and High Sensitivity Cw-Cavity Ringdown Absorption Spectroscopies of Ozone in the 6030-6130 Cm-1 Region. First Observation and Analysis of the 3ν1+3ν3 and 2ν2+5ν3 Bands." Journal of Molecular Structure 780–781(SPEC. ISS.):225–33. doi: 10.1016/j.molstruc.2005.06.051.

[De Backer-Barilli2012]
De Backer-Barilly, M. R., A. Barbe, E. Starikova, Vl G. Tyuterev, S. Kassi, and A. Campargue. 2012. "Detection and Analysis of Four New Bands in CRDS 16O 3 Spectra between 7300 and 7600 Cm -1." Journal of Molecular Spectroscopy 272(1):43–50. doi: 10.1016/j.jms.2012.01.001.

[Barbe2007a]
Barbe, A., M. R. De Backer-Barilly, Vl G. Tyuterev, A. Campargue, D. Romanini, and S. Kassi. 2007. "CW-Cavity Ring Down Spectroscopy of the Ozone Molecule in the 5980-6220 Cm-1 Region." Journal of Molecular Spectroscopy 242(2):156–75. doi: 10.1016/j.jms.2007.02.022.

[Barbe2007b]
Barbe, A., M. R. De Backer-Barilly, Vl G. Tyuterev, S. Kassi, and A. Campargue. 2007. "CW-Cavity Ring down Spectroscopy of the Ozone Molecule in the 6220-6400 Cm-1 Region." Journal of Molecular Spectroscopy 246(1):22–38. doi: 10.1016/j.jms.2007.08.001.

[Barbe2011]
Barbe, A., M. R. De Backer-Barilly, Vl G. Tyuterev, S. Kassi, and A. Campargue. 2011. "Detection and Analysis of New Bands of 16O3 by CRDS between 6500 and 7300 Cm-1." Journal of Molecular Spectroscopy 269(2):175–86. doi: 10.1016/j.jms.2011.06.005.

[Barbe2013]
Barbe, A., S. Mikhailenko, E. Starikova, M. R. De Backer, Vl G. Tyuterev, D. Mondelain, S. Kassi, A. Campargue, C. Janssen, S. Tashkun, R. Kochanov, R. Gamache, and J. Orphal. 2013. "Ozone Spectroscopy in the Electronic Ground State: High-Resolution Spectra Analyses and Update of Line Parameters since 2003." Journal of Quantitative Spectroscopy and Radiative Transfer 130:172–90. doi: 10.1016/j.jqsrt.2013.06.007.

[Bouvier1998]
Bouvier, A. J., D. Inard, V. Veyret, B. Bussery, R. Bacis, S. Churassy, J. Brion, J. Malicet, and R. H. Judge. 1998. "Contribution to the Analysis of the 3A2 ← X1A1 'Wulf' Transition of Ozone by High-Resolution Fourier Transform Spectrometry." Journal of Molecular Spectroscopy 190(2):189–97. doi: 10.1006/jmsp.1998.7578.

[Bouvier1999]

Bouvier, A. J., V. Veyret, I. Russier, D. Inard, S. Churassy, R. Bacis, J. Brion, J. Malicet, and R. H. Judge. 1999. "Comparative Rotational Analysis of the 000 Bands of the 3A2←X1A1 Wulf Transition for the Isotopomers 16O3 and 18O3 of Ozone by High Resolution Fourier Transform Spectrometry." Spectrochimica Acta - Part A: Molecular and Biomolecular Spectroscopy 55(14):2811–21. doi: 10.1016/S1386-1425(99)00096-7.

[Braunstein1995]
Braunstein, M., R. L. Martin, and P. J. Hay. 1995. "Investigation of the Role of Triplet States in the Wulf Bands of Ozone." The Journal of Chemical Physics 102(9):3662–66. doi: 10.1063/1.468595.

[Campargue2008]
Campargue, A., A. Barbe, M. R. De Backer-Barilly, Vl G. Tyuterev, and S. Kassi. 2008. "The near Infrared Spectrum of Ozone by CW-Cavity Ring down Spectroscopy between 5850 and 7000 Cm-1: New Observations and Exhaustive Review." Physical Chemistry Chemical Physics 10(20):2925–46. doi: 10.1039/b719773j.

[Campargue2015]
Campargue, A., S. Kassi, D. Mondelain, A. Barbe, E. Starikova, M. R. De Backer, and Vl G. Tyuterev. 2015. "Detection and Analysis of Three Highly Excited Vibrational Bands of 16O3 by CW-CRDS near the Dissociation Threshold." Journal of Quantitative Spectroscopy and Radiative Transfer 152:84–93. doi: 10.1016/j.jqsrt.2014.10.019.

[Campargue2006]
Campargue, A., S. Kassi, D. Romanini, A. Barbe, M. R. De Backer-Barilly, and Vl G. Tyuterev. 2006. "CW-Cavity Ring down Spectroscopy of the Ozone Molecule in the 6625-6830 Cm-1 Region." Journal of Molecular Spectroscopy 240(1):1–13. doi: 10.1016/j.jms.2006.07.010.

[Charlo2004]
Charlo, David, and David C. Clary. 2004. "Quantum-Mechanical Calculations on Pressure and Temperature Dependence of Three-Body Recombination Reactions: Application to Ozone Formation Rates." Journal of Chemical Physics 120(6):2700–2707. doi: 10.1063/1.1635361.

[Fabian2014]
P. Fabian and M. Dameris, 2014. Ozone in the Atmosphere: Basic Principles, Natural and Human Impacts. Springer Berlin Heidelberg. p. 137. doi: 10.1007/978-3-642-54099-8. ISBN. 9783642540998

[Feilberg2013]
Feilberg, K. L., A. A. Wiegel, and K. A. Boering. 2013. "Probing the Unusual Isotope Effects in Ozone Formation: Bath Gas and Pressure Dependence of the Non-Mass-Dependent Isotope Enrichments in Ozone." Chemical Physics Letters 556:1–8. doi: 10.1016/j.cplett.2012.10.038.

[Gordon2017]
Gordon, I. E., L. S. Rothman, C. Hill, R. V. Kochanov, Y. Tan, P. F. Bernath, M. Birk, V. Boudon, A. Campargue, K. V. Chance, B. J. Drouin, J. M. Flaud, R. R. Gamache, J. T. Hodges, D. Jacquemart, V. I. Perevalov, A. Perrin, K. P. Shine, M. A. H. Smith, J. Tennyson, G. C. Toon, H. Tran, V. G. Tyuterev, A. Barbe, A. G. Császár, V. M. Devi, T. Furtenbacher, J. J. Harrison, J. M. Hartmann, A. Jolly, T. J. Johnson, T. Karman, I. Kleiner, A. A. Kyuberis, J. Loos, O. M. Lyulin, S. T. Massie, S. N. Mikhailenko, N. Moazzen-Ahmadi, H. S. P. Müller, O. V. Naumenko, A. V. Nikitin, O. L. Polyansky, M. Rey, M. Rotger, S. W. Sharpe, K. Sung, E. Starikova, S. A. Tashkun, J. Vander Auwera, G. Wagner, J. Wilzewski, P. Wcisło, S. Yu, and E. J. Zak. 2017. "The HITRAN2016 Molecular Spectroscopic Database." Journal of Quantitative Spectroscopy and Radiative Transfer 203:3–69. doi: 10.1016/j.jqsrt.2017.06.038.

[Grebenshchikov2007]
Grebenshchikov, S. Yu, Z. W. Qu, H. Zhu, and R. Schinke. 2007. "New Theoretical Investigations of the Photodissociation of Ozone in the Hartley, Huggins, Chappuis, and Wulf Bands." Physical Chemistry Chemical Physics 9(17):2044–64. doi: 10.1039/b701020f

[Griggs1968]
Griggs, M. 1968. "Absorption Coefficients of Ozone in the Ultraviolet and Visible Regions." The Journal of Chemical Physics 49(2):857–59. doi: 10.1063/1.1670152.

[Guillon2018]
Guillon, Grégoire, Pascal Honvault, Roman Kochanov, and Vladimir Tyuterev. 2018. “First-Principles Computed Rate Constant for the O + O2 Isotopic Exchange Reaction Now Matches Experiment.” Journal of Physical Chemistry Letters 9(8):1931–36. doi: 10.1021/acs.jpclett.8b00661.

[Holka2010]
Holka, Filip, Péter G. Szalay, Thomas Müller, and Vladimir G. Tyuterev. 2010. “Toward an Improved Ground State Potential Energy Surface of Ozone.” Journal of Physical Chemistry A 114(36):9927–35. doi: 10.1021/jp104182q.

[Inard1998]
Inard, D., A. J. Bouvier, R. Bacis, S. Churassy, F. Bohr, J. Brion, J. Malicet, and M. Jacon. 1998. “Absorption Cross-Sections and Lifetime of the 3A2 ‘metastable’ State of Ozone.” Chemical Physics Letters 287(5–6):515–24. doi: 10.1016/S0009-2614(98)00200-0.

[Janssen2003]
Janssen, C., J. Guenther, D. Krankowsky, and K. Mauersberger. 2003. “Temperature Dependence of Ozone Rate Coefficients and Isotopologue Fractionation in 16O-18O Oxygen Mixtures.” Chemical Physics Letters 367(1–2):34–38. doi: 10.1016/S0009-2614(02)01665-2.

[Karlovets2021]
Karlovets, E. V., S. Kassi, S. A. Tashkun, and A. Campargue. 2021. “The Absorption Spectrum of Nitrous Oxide between 8325 and 8622 Cm−1.” Journal of Quantitative Spectroscopy and Radiative Transfer 262:107508. doi: 10.1016/j.jqsrt.2021.107508.

[Kassi2007]
Kassi, S., A. Campargue, M. R. De Backer-Barilly, and A. Barbe. 2007. “The N1 + 3ν2 + 3ν3 and 4ν1 + N2 + N3 Bands of Ozone by CW-Cavity Ring down Spectroscopy between 5900 and 5960 Cm-1.” Journal of Molecular Spectroscopy 244(2):122–29. doi: 10.1016/j.jms.2007.05.012.

[Kassi2012]
Kassi, Samir, and Alain Campargue. 2012. “Cavity Ring down Spectroscopy with 5 × 10 −13 Cm −1 Sensitivity.” The Journal of Chemical Physics 137(23):234201. doi: 10.1063/1.4769974.

[Kokoouline2020]
Kokoouline, Viatcheslav, David Lapierre, Alexander Alijah, and Vladimir Tyuterev. 2020. “Localized and Delocalized Bound States of the Main Isotopologue 48O3and of 18O-Enriched 50O3isotopomers of the Ozone Molecule near the Dissociation Threshold.” Physical Chemistry Chemical Physics 22(28):15885–99. doi: 10.1039/d0cp02177f.

[Konefał2020]
Konefał, Magdalena, Samir Kassi, Didier Mondelain, and Alain Campargue. 2020. “High Sensitivity Spectroscopy of the O2 Band at 1.27 Mm: (I) Pure O2 Line Parameters above 7920 Cm−1.” Journal of Quantitative Spectroscopy and Radiative Transfer 241:106653. doi: 10.1016/j.jqsrt.2019.106653.

[Lapierre2016]
Lapierre, David, Alexander Alijah, Roman Kochanov, Viatcheslav Kokoouline, and Vladimir Tyuterev. 2016. “Lifetimes and Wave Functions of Ozone Metastable Vibrational States near the Dissociation Limit in a Full-Symmetry Approach.” Physical Review A 94(4):042514. doi: 10.1103/PhysRevA.94.042514.

[Lu2009]
Lu, Q. B. 2009. “Correlation between Cosmic Rays and Ozone Depletion.” Physical Review Letters 102(11):118501. doi: 10.1103/PhysRevLett.102.118501.

[Minaev1994]
Minaev, Boris, and Hans Ågren. 1994. “The Interpretation of the Wulf Absorption Band of Ozone.” Chemical Physics Letters 217(5–6):531–38. doi: 10.1016/0009-2614(93)E1445-M.

[Mondelain2013]
Mondelain, D., A. Campargue, S. Kassi, A. Barbe, E. Starikova, M. R. De Backer, and Vl G. Tyuterev. 2013. “The CW-CRDS Spectra of the 16O/18O Isotopologues of Ozone between 5930 and 6340cm-1-Part 1: 16O16O18O.” Journal of Quantitative Spectroscopy and Radiative Transfer 116:49–66. doi: 10.1016/j.jqsrt.2012.10.023.

[Mondelain2012]
Mondelain, Didier, Rémy Jost, Samir Kassi, Richard H. Judge, Vladimir Tyuterev, and Alain Campargue. 2012. “Predissociation and Spectroscopy of the 3A 2(000) State of 18O 3 from CRDS Spectra of the 3A 2(000)←X 1A 1(110) Hot Band near 7900cm -1.” Journal of Quantitative Spectroscopy and Radiative Transfer 113(11):840–49. doi: 10.1016/j.jqsrt.2012.01.015.

[Mondelain2011]
Mondelain, Didier, Samir Kassi, Rémy Jost, and Alain Campargue. 2011. “The High Sensitivity Absorption Spectrum of Ozone (18O 3 and 16O3) near 7800 Cm-1: Identification of the 3A2(0 0 0)-X(1 1 0) Hot Band Superimposed to Very Weak Vibrational Bands.” Chemical Physics Letters 510(4–6):191–96. doi: 10.1016/j.cplett.2011.05.043.

[Rosmus2002]
Rosmus, Pavel, Paolo Palmieri, and Reinhard Schinke. 2002. “The Asymptotic Region of the Potential Energy Surfaces Relevant for the O(3P)+O2(X3Σg-) ⇌O3 Reaction.” Journal of Chemical Physics 117(10):4871–77. doi: 10.1063/1.1491396.

[Ruscic2010]
Ruscic, B. 2010. “Unpublished Results Obtained from Active Thermochemical Tables (ATcT) Based on the Core (Argonne), Thermochemical Network Version 1.110.”

[Schinke2006]
Schinke, R., S. Yu. Grebenshchikov, M. V. Ivanov, and P. Fleurat-Lessard. 2006. “DYNAMICAL STUDIES OF THE OZONE ISOTOPE EFFECT: A Status Report.” Annual Review of Physical Chemistry 57(1):625–61. doi: 10.1146/annurev.physchem.57.032905.104542.

[Serdyuchenko2014]
Serdyuchenko, A., V. Gorshelev, M. Weber, W. Chehade, and J. P. Burrows. 2014. “High Spectral Resolution Ozone Absorption Cross-Sections – Part 2: Temperature Dependence.” Atmospheric Measurement Techniques 7(2):625–36. doi: 10.5194/amt-7-625-2014.

[Starikov2011]
Starikov, V. I. 2011. “Calculation and Analytical Representation of Self-Pressure and Air Pressure Broadening Coefficients of Ozone Spectral Lines.” Optics and Spectroscopy (English Translation of Optika i Spektroskopiya) 110(3):340–50. doi: 10.1134/S0030400X11030222.

[Starikova2015]
Starikova, E., D. Mondelain, A. Barbe, Vl G. Tyuterev, S. Kassi, and A. Campargue. 2015. “CRDS Detection and Modelling of Vibrational Bands of 18O3 Approaching the Dissociation Threshold (7400-7920cm-1).” Journal of Quantitative Spectroscopy and Radiative Transfer 161:203–14. doi: 10.1016/j.jqsrt.2015.04.001.

[Tyuterev2000]
Tyuterev, Vl G., S. A. Tashkun, D. W. Schwenke, P. Jensen, T. Cours, A. Barbe, and M. Jacon. 2000. “Variational EKE-Calculations of Rovibrational Energies of the Ozone Molecule from an Empirical Potential Function.” Chemical Physics Letters 316(3–4):271–79. doi: 10.1016/S0009-2614(99)01228-2.

[Tyuterev2013]
Tyuterev, Vladimir G., Roman V. Kochanov, Sergey A. Tashkun, Filip Holka, and Péter G. Szalay. 2013. “New Analytical Model for the Ozone Electronic Ground State Potential Surface and Accurate Ab Initio Vibrational Predictions at High Energy Range.” Journal of Chemical Physics 139(13):134307. doi: 10.1063/1.4821638.

[Tyuterev2014]

Tyuterev, Vl G., R. Kochanov, A. Campargue, S. Kassi, D. Mondelain, A. Barbe, E. Starikova, M. R. De Backer, P. G. Szalay, and S. Tashkun. 2014. “Does the ‘Reef Structure’ at the Ozone Transition State towards the Dissociation Exist? New Insight from Calculations and Ultrasensitive Spectroscopy Experiments.” Physical Review Letters 113(14):143002. doi: 10.1103/PhysRevLett.113.143002.

[Vasilchenko2020]
Vasilchenko, Semen, Alain Barbe, Evgeniya Starikova, Samir Kassi, Didier Mondelain, Alain Campargue, and Vladimir Tyuterev. 2020. “Detection and Assignment of Ozone Bands near 95% of the Dissociation Threshold: Ultrasensitive Experiments for Probing Potential Energy Function and Vibrational Dynamics.” Physical Review A 102(5):052804. doi: https://doi.org/10.1103/PhysRevA.102.052804.

[Wachsmuth2003]
Wachsmuth, Uwe, and Bernd Abel. 2003. “Linewidths and Line Intensity Measurements in the Weak 3A2(000) ← X̃1 A1(000) Band of Ozone by Pulsed Cavity Ringdown Spectroscopy.” Journal of Geophysical Research D: Atmospheres 108(15):4473. doi: 10.1029/2002jd003126.

[Xie2001]
Xie, Daiqian, Hua Guo, and Kirk A. Peterson. 2001. “Ab Initio Characterization of Low-Lying Triplet State Potential-Energy Surfaces and Vibrational Frequencies in the Wulf Band of Ozone.” Journal of Chemical Physics 115(22):10404–8. doi: 10.1063/1.1417502.

[Xie2005]
Xie, Tiao, and Joel M. Bowman. 2005. “Quantum Inelastic Scattering Study of Isotope Effects in Ozone Stabilization Dynamics.” Chemical Physics Letters 412(1–3):131–34. doi: 10.1016/j.cplett.2005.06.111.

[Yuen2019]
Yuen, Chi Hong, David Lapierre, Fabien Gatti, Viatcheslav Kokoouline, and Vladimir G. Tyuterev. 2019. “The Role of Ozone Vibrational Resonances in the Isotope Exchange Reaction 16O16O + 18O → 18O16O + 16O: The Time-Dependent Picture.” Journal of Physical Chemistry A 123(36):7733–43. doi: 10.1021/acs.jpca.9b06139.